First results of the LHC Longitudinal Density Monitor

A. Jeff [a,b]; A. Boccard[a]; E. Bravin[a]; A.S.Fisher[c]; T. Lefèvre[a]; A. Rabiller[a]; F. Roncarolo[a]; C.P. Welsch[b,d].

[a] CERN, Geneva, CH
[b] University of Liverpool, Liverpool, UK
[c] SLAC, Menlo Park, CA, USA
[d] Cockcroft Institute, Daresbury, UK

Summary

The Large Hadron Collider (LHC) at CERN is the world's largest particle accelerator. It is designed to accelerate and collide protons or heavy ions up to the center-of-mass energies of 14TeV. Knowledge of the longitudinal distribution of particles is important for various aspects of accelerator operation, in particular to check the injection quality and to measure the proportion of charge outside the nominally filled bunches during the physics periods. In order to study this so-called ghost charge at levels very much smaller than the main bunches, a longitudinal profile measurement with a very high dynamic range is needed. A new detector, the LHC Longitudinal Density Monitor (LDM) is a single-photon counting system measuring synchrotronlight by means of an avalanche photodiode detector. The unprecedented energies reached in the LHC allow synchrotronlight diagnostics to be used with both protons and heavy ions. A prototype was installed during the 2010 LHC run and was able to longitudinally profile the whole ring with a resolution close to the target of 50 ps. On-line correction for the effects of the detector deadtime, pile-up and afterpulsing allow a dynamic range of 10^5 to be achieved. First measurements with the LDM are presented here along with an analysis of its performance and an outlook for future upgrades.

First results of the LHC longitudinal density monitor

A. Jeff [a,b,*], A. Boccardi [a], E. Bravin [a], A.S. Fisher [c], T. Lefevre [a], A. Rabiller [a], F. Roncarolo [a], C.P. Welsch [b,d]

[a] CERN, Geneva, Switzerland
[b] University of Liverpool, Liverpool, UK
[c] SLAC, Menlo Park, CA, USA
[d] Cockcroft Institute, Daresbury, UK

ARTICLE INFO

ABSTRACT

The Large Hadron Collider (LHC) at CERN is the world's largest particle accelerator. It is designed to accelerate and collide protons or heavy ions up to the center-of-mass energies of 14 TeV.

Knowledge of the longitudinal distribution of particles is important for various aspects of accelerator operation, in particular to check the injection quality and to measure the proportion of charge outside the nominally filled bunches during the physics periods. In order to study this so-called ghost charge at levels very much smaller than the main bunches, a longitudinal profile measurement with a very high dynamic range is needed.

A new detector, the LHC Longitudinal Density Monitor (LDM) is a single-photon counting system measuring synchrotron light by means of an avalanche photodiode detector. The unprecedented energies reached in the LHC allow synchrotron light diagnostics to be used with both protons and heavy ions.

A prototype was installed during the 2010 LHC run and was able to longitudinally profile the whole ring with a resolution close to the target of 50 ps. On-line correction for the effects of the detector deadtime, pile-up and afterpulsing allow a dynamic range of 10^5 to be achieved.

First measurements with the LDM are presented here along with an analysis of its performance and an outlook for future upgrades.

© 2011 Elsevier B.V. All rights reserved.

1. Introduction

The LHC at CERN is the world's largest particle accelerator and is designed to accelerate and collide beams of either protons or heavy ions [1]. The particle decays observed in the LHC experiments after these collisions will further our understanding of the universe, potentially confirming the existence of theoretically predicted particles such as the Higgs boson or revealing new physics that goes beyond the Standard Model.

Particle beams are injected into the LHC at 450 GeV for protons and at an equivalent energy for heavy ions. In 2010 fully stripped lead ions were used ($Z=82$, $A=208$) leading to an injection energy per nucleon of $450\,\text{GeV} \times Z/A = 177\,\text{GeV}$ (Table 1). A sequence of pre-existing accelerators known as the LHC injector chain is used to accelerate the beam to this energy. The LHC injector chain for protons consists of the Linac 2, Proton Synchrotron Booster (PSB), Proton Synchrotron (PS) and Super Proton Synchrotron (SPS) [2] while for heavy ions Linac 3 and the Low Energy Ion Ring (LEIR) replace Linac 2 and the booster, respectively [3]. At the end of each stage, fast-rising kicker magnets are used to direct the beam to the next accelerator. To prevent any particles from receiving a partial kick, gaps must be left in the filling pattern so that each kicker can fire whilst it is empty of particles. Similarly, a fast kicker is used to redirect the LHC beam down a dump line when it is no longer wanted, in the case of equipment malfunction or if abnormal beam losses are detected. The gap left for the risetime of the LHC dump kicker is 3 µs long and is known as the abort gap. Fig. 1 shows the injector chain while Fig. 2 shows the constraints it imposes on the nominal LHC filling pattern. Each bunch lies inside an RF bucket 2.5 ns long, but at most 1 in 10 of the 35,640 RF buckets are foreseen to be filled with a bunch, with additional gaps as explained above.

However, a small proportion of the beam can be accidentally injected into adjacent buckets forming satellite bunches. These satellites can be located one or more buckets away from the main bunch, depending on where in the injector chain they originate. Once formed, the satellites are steered, focused and accelerated like main bunches.

In addition, some particles that have too high or too low a momentum are not trapped in a bucket. This 'debunched' beam then drifts from bucket to bucket until it is lost or recaptured into

* Corresponding author at: CERN, CH-1211, Geneva 23, Switzerland.
Tel.: +41 22 76 77179; fax +41 22 76 69870.
E-mail address: adam.jeff@cern.ch (A. Jeff).

a bucket. If recaptured it forms very small ghost bunches, which can be spread around the whole ring.

These satellite and ghost bunches can collide at the interaction points either against each other or with a main bunch and create background noise for the experiments. In addition, they cause problems in the calibration of other instruments, and in extreme

Table 1
Summary of some key LHC parameters.

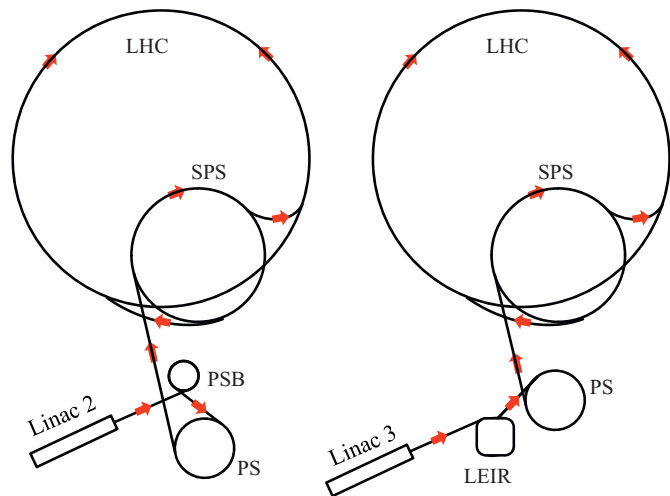|	Protons	Lead ions
Maximum beam energy (2010)	3.5 TeV	3.5×82 TeV/ion
Revolution frequency	11.2 kHz	
RF frequency	400.8 MHz	
Minimum bunch spacing	24.95 ns	100 ns
Maximum number of bunches	2808	592
Bunch population (ultimate)	1.7×10^{11}	8.2×10^9 charges [10^8 ions]
Longitudinal emittance (injection)	0.7 eV s	
Longitudinal emittance (during physics)	1.75 eV s	

Fig. 1. Schematic of the LHC injector chain for protons (left) and heavy ions (right).

cases could damage the machine, especially if a high enough population were to enter the abort gap. It is therefore very important to know the level and distribution of these ghost and satellite bunches.

Synchrotron Radiation (SR) is an excellent tool for particle beam diagnostics as it is non-disruptive and carries information on both the transverse and longitudinal particle distributions. It is widely used in electron storage rings [4,5], where the SR intensities are very high. Since the SR power emitted is proportional to the fourth power of the relativistic γ, the intensity of SR from a proton beam is 13 orders of magnitude lower than that of an electron beam with the same energy and the same radius of curvature. Nonetheless, synchrotron radiation has been used for diagnostics at the highest-energy proton accelerators [6,7].

A number of methods exist to convert synchrotron light into longitudinal profiles. For example, streak cameras [8] have excellent time resolution down to the picoseconds scale [9]; however the dynamic range is limited and the record length is much shorter than the 89 μs required to cover the full LHC ring. Non-linear mixing of the synchrotron light with light from a pulsed laser can also produce longitudinal profiles with excellent time resolution and high dynamic range [10], but due to the low conversion efficiency of the non-linear process this method suffers from a low signal-to-noise ratio if the SR intensity is low, which is the case with the LHC at injection energy. Single photon counting (SPC) [11] is a relatively low-cost solution that is capable of measuring the full LHC ring with high dynamic range. SPC can also provide over an order of magnitude improvement when compared to electromagnetic measurements of the beam using wall current monitors (WCM) [12] or beam current transformers (BCT) [13], where the dynamic range is usually limited by acquisition noise and imperfections introduced due to impedance mismatch.

2. Principle of the detector

Single-photon counting is used in order to achieve a high dynamic range. This is illustrated schematically in Fig. 3. Each particle bunch passes the LDM once in every revolution (turn), emitting synchrotron radiation. The light level is adjusted such that
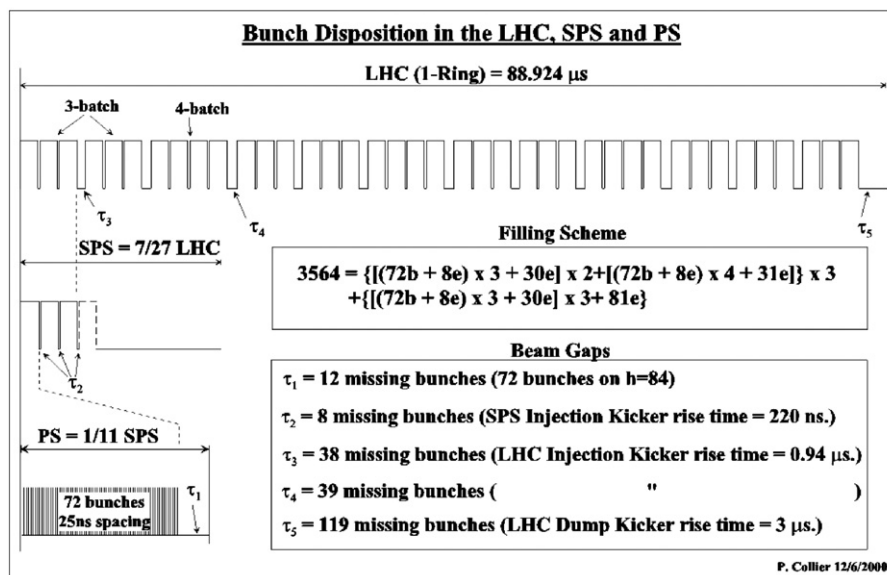

Fig. 2. Ultimate LHC filling scheme for protons. Gaps are left to allow for injection and extraction in the LHC's injection chain, as well as to allow for the LHC dump kicker.
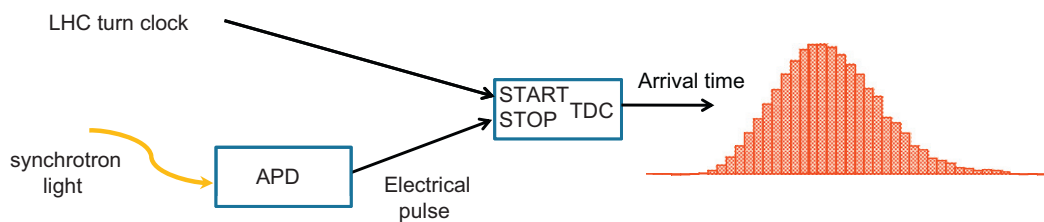
Fig. 3. Schematic of the Longitudinal Density Monitor system. Single photons of synchrotron light are detected by an avalanche photodiode (APD) and their arrival times are recorded by a time-to-digital converter (TDC). The arrival times are histogrammed to build up a longitudinal profile over many turns.

Table 2
Key wavelengths of SR emission in the LHC BSRT system. SR from the dipole has a very broad spectrum, characterized by the critical wavelength, which is the median wavelength of emission (equal power is radiated above and below this wavelength). SR from the undulator is emitted primarily at the undulator wavelength and its harmonics, but this spectrum is also significantly broadened because the undulator has only 2 periods.

Beam Energy	Undulator wavelength	Dipole critical wavelength
Protons		
450 GeV	609 nm	228 μm
3.5 TeV	10 nm	484 nm
Lead Ions		
450Z GeV	3.9 μm	3.7 mm
3.5Z TeV	65 nm	7.9 μm

the probability of detecting a photon from the bunch is much less than one for each passage. The avalanche photodiode (APD) detects the incoming photon and produces a corresponding electrical pulse. This is time-stamped by a time-to-digital converter (TDC). A multi-stop TDC is used allowing many photons to be counted during each LHC revolution. A histogram of photon arrival times can then be created with data collected over thousands of turns. The longer the acquisition, the more the counts added to the histogram, and the higher the dynamic range of the measurement.

SR is emitted with a broad spectrum, but only the visible part is used for the LDM. The synchrotron light for the LDM comes from two sources. A dipole with a maximum field of 3.9 T emits visible SR at beam energies above 1.5 TeV, but produces only infra-red radiation at the injection energy of 0.45 TeV. To fill this gap a superconducting undulator with two 28 cm periods and a peak field of 5 T was installed upstream of the dipole. The undulator produces visible light from 0.45 to 1.5 TeV before moving into the ultraviolet above 1.5 TeV. Visible light is thus available across the whole LHC energy range, with a minimum intensity at the crossover of the two sources around 1.2 TeV [14]. When the LHC is operated with lead ions, γ is smaller and the undulator radiation is mainly in the IR at the injection energy of 177 GeV per nucleon. The visible light emitted is then at a minimum at injection and rises steadily with energy (Table 2). The variation in intensity was calculated using the simulation code SRW [15] and is shown in Fig. 4, along with the intensity measured during the energy ramp by a photomultiplier tube gated on a single bunch. The simulation agrees well with the relative intensity change observed.

Due to the very large radius of curvature of the LHC, the angle between the SR and proton beams at the exit of the dipole is just 1.5 mrad. Only some 30 m downstream of the undulator is the separation sufficient to allow an extraction mirror to be inserted and the SR is then sent out of the beampipe through a silica window. Because of the distance from the source, an arrangement of mirrors known as the Beam Synchrotron Radiation Telescope

(BSRT) is installed to focus the light [16]. A motorized 'trombone' is used to vary the optical path length and thus move the focus between the undulator and the dipole. The light is split four ways, with the LDM receiving about 7% of the total and the rest used for fast and slow transverse profiling [17] and abort gap monitoring [18]. Each monitor has a remotely controllable neutral-density filter wheel for independent intensity control. The arrangement is shown schematically in Fig. 5. A separate but identical system is installed for each of the two LHC beams.

Because the source of SR is spread over more than 4 m (from the entrance of the undulator to the point in the dipole at which it leaves the angular acceptance of the BSRT), some time slippage can occur between particles and photons. This slippage occurs due to both path length and velocity differences, and means that the SR pulse is slightly stretched compared to the emitting bunch. However, this effect has been calculated (following [19]) to be no more than 0.25 ps in this arrangement, and is thus negligible compared to the resolution of the instrument. In addition, the use of all-reflective optics minimizes dispersion. The dispersion in the window through which SR exits the beam pipe is estimated to be 2.2 ps based on light between 300 nm and 850 nm passing through 20 mm of fused silica.

The detector used for the LDM is the Photon Detection Module (PDM) from Micro Photon Devices [20]. This is a silicon APD operated in the Geiger mode [21] and is sensitive between approximately 350 and 850 nm. The detection efficiency is $\sim$35% averaged over the visible range, however the active area of the APD is only 50 μm and this leads to a substantial coupling loss. The time resolution is 50 ps FWHM. The PDM uses an active quenching circuit to reduce the voltage across the APD as soon as an avalanche is detected. The voltage is kept below breakdown for a certain period, known as the deadtime, during which the detector is blind to any further photons. The PDM has a deadtime of 77 ns. At the end of the deadtime the voltage is restored and at this point there is an increased chance of a false count occurring due to charge carriers having become trapped in the silicon. These correlated false counts, known as afterpulses, occur with a probability of approximately 3% after each avalanche, and so dominate over uncorrelated dark counts, which occur with a much lower rate.

The TDC used is an Acquiris TC890 (also called Agilent U1051A) [22], which has a minimum bin width of 50 ps. A START pulse is provided at the LHC revolution frequency by the Beam Synchronous Timing system [23]. The STOP signals are the electrical pulses generated by the PDM and carried over $\sim$50 m of coaxial cable to the TDC, which is located in a radiation-free electronics area outside the LHC tunnel. The TC890 is a multi-stop TDC so that the time stamps of many STOP pulses can be given relative to each START. The minimum separation of two STOPs is 15 ns; since this is smaller than the deadtime of the PDM it will have no effect on the measurements. The maximum average count rate is limited to 20 Mhits/s by the maximum data read-out rate.
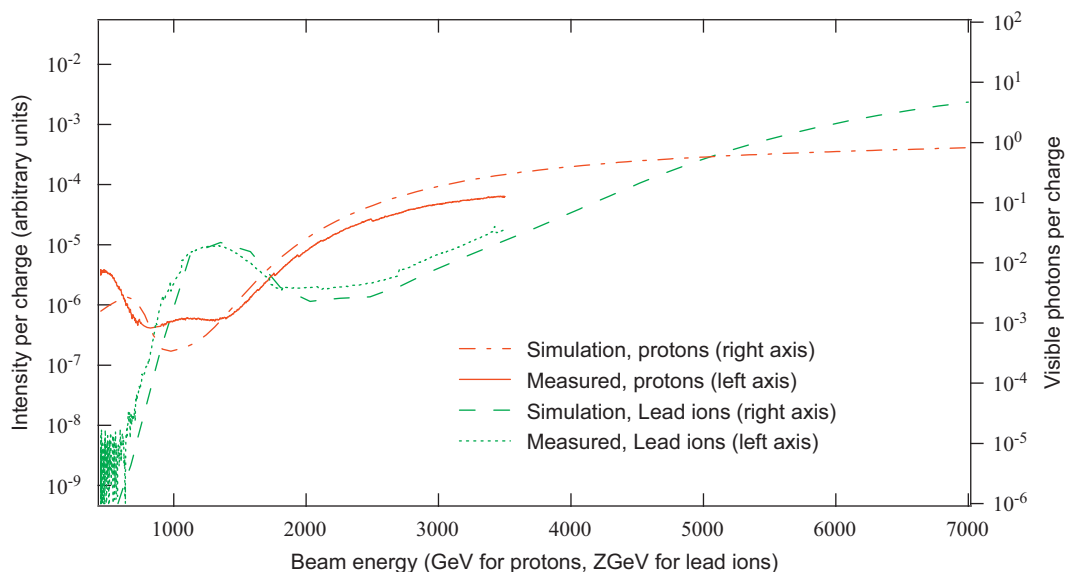
Fig. 4. Probability of each beam charge emitting an SR photon within the geometrical acceptance and the wavelength range of the detector, as a function of beam energy. The measured values agree well with simulations.
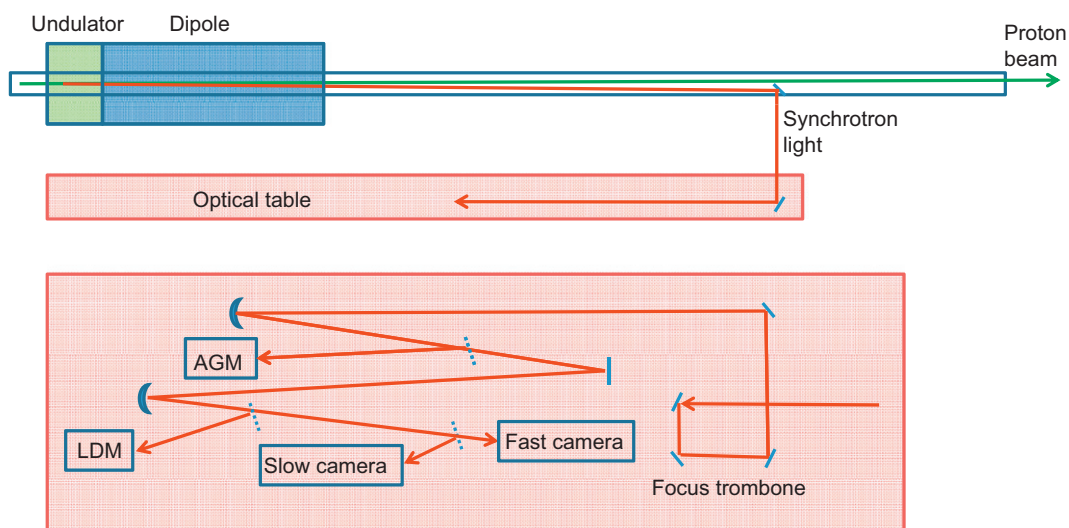

Fig. 5. Simplified schematic of the Beam Synchrotron Radiation Telescope (BSRT). Above, side view. Below, top view of the optical table. Some components are omitted for clarity, e.g. filter wheels.

3. Correction for deadtime and afterpulses

An APD operated in Geiger mode has a certain deadtime due to the need to quench the avalanches. As well as limiting the maximum count rate, this introduces a distortion to the pulse shape. If a photon is detected from the first part of the pulse, the detector will be blind to any further photons. The measured pulse is thus skewed towards earlier times. In typical single-photon counting applications, the count rate is kept so low that this effect is negligible. However, in order to keep the integration time to a minimum it is desirable to have a higher count rate, and thus correction for the effect of deadtime is necessary.

In order to correct the number of counts in bin i, the total number of counts in the previous 77 ns of the histogram is found, and divided by the number of turns that were integrated over. This gives the probability that the APD was in deadtime during

bin i. A correction can then be calculated as

$$C_i = \frac{x_i}{P(ready)_i} = x_i \frac{N}{N - \sum_{j=i-d}^{i-1} x_j}$$

where x_i is the number of photons counted in bin i over N turns, d is the deadtime in bins and C_i is the number of photons, which would be counted by a detector with no deadtime [24].

This procedure was tested in the laboratory using a pulsed LED as the light source. The pulse shape was measured with a high arrival rate (>1 photon per pulse) and the correction applied. A neutral density filter with transmission of 0.01% was then placed in front of the detector and the pulse shape measured again. In this case the count rate was low enough to make the deadtime effect negligible and no correction was applied. As shown in Fig. 6, the two measurements agree closely.
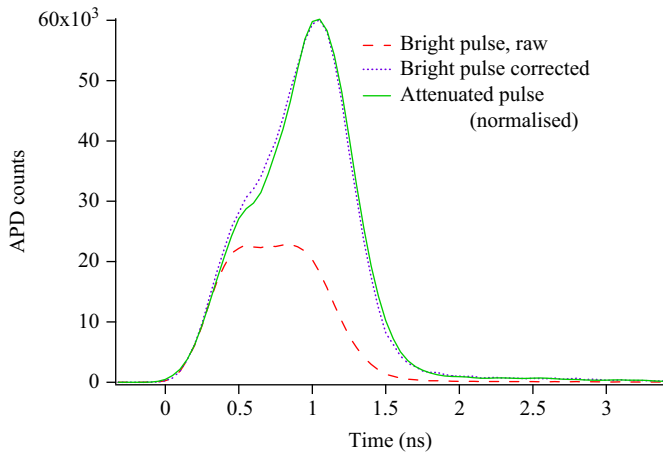
Fig. 6. Skew due to deadtime can be compensated with an appropriate correction algorithm. Here a pulsed LED is used to test the correction procedure. For the bright pulse the arrival rate was 2 countable photons per pulse (allowing for the quantum efficiency of the detector). The raw measurement shows that the pulse shape is considerably misrepresented; the correct pulse shape is restored after correction.

At the end of the deadtime, when the APD's operating voltage is restored, it has an increased chance of producing a spontaneous avalanche or afterpulse [25]. This is caused by the presence of charge carriers trapped in impurities in the silicon. Especially when they are absorbed outside the active layer of the device, these trapped charges can have a lifetime much longer than the deadtime, and can therefore be released after the operating voltage has been restored, causing an avalanche, which is indistinguishable from one caused by an incident photon. These afterpulses are most likely to occur at the end of the deadtime but can spread over several µs, with probability decreasing further from the original hit [26]. The decay in afterpulse probability in the LDM has been found experimentally to be best fitted by multiple exponentials, with the main components having time constants of 25 and 45 ns. The afterpulses can therefore be statistically eliminated by subtraction of a sequence of infinite impulse response filters.

A third correction is applied to account for the possibility of two photons arriving during the same bin. The probability of this occurring is small but not negligible for the peak bins of each bunch. Since the two photons produce only one count, the effect is to slightly flatten the peak. The arriving photons follow a Poisson distribution, so the appropriate correction is

$$P_i = -\ln(1 - C_i/N)$$

where P_i is the number of photons emitted during bin i, which is directly proportional to the particle density.

A Monte Carlo simulation has been made to check the accuracy of this correction algorithm and to optimize the parameters of the system. The correction was found to be effective up to a count rate of several photons per bunch. However, the optimum count rate for high-dynamic-range operation was shown to be 0.5 counts per deadtime period; that is 0.125 photons per bunch for the minimum bunch spacing of 25 ns and deadtime of 77 ns. A higher count rate leads to too much distortion, while a lower rate reduces the dynamic range that can be achieved with a given integration time.

Another interesting result from the simulation is that the correction becomes noisier if the deadtime is equal to the bunch spacing or a multiple thereof. Unfortunately, the only suitable APD modules commercially available have deadtimes of 45 ns and 77 ns, close to the 50 ns and 75 ns bunch spacing used in the LHC respectively.

4. Results

Measurements were taken with the LDM during both LHC proton and lead ion runs. In the case of lead ions, the lower relativistic γ means thatSR is almost entirely in the infra-red at injection, and measurements with LDM were possible only above 350 GeV per nucleon (equivalent to 900 GeV for protons). An example of a measured profile is shown in Fig. 7 with the full profile containing some 1.8 million bins. In this case, a long integration time of several hundred seconds (several million turns) was used in order to make a high-dynamic range profile showing satellites, but profiles showing only main bunches can be made in approximately 10 s.
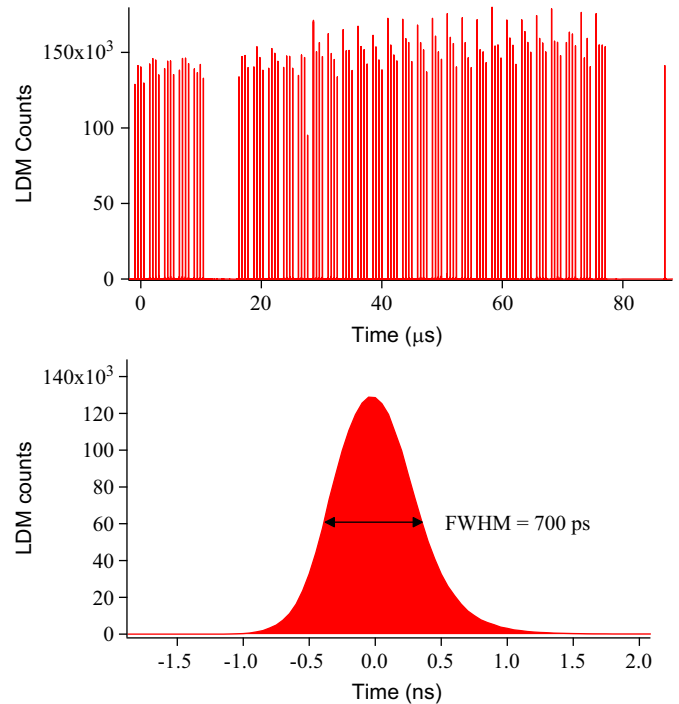

Fig. 7. Longitudinal profile obtained during an LHC lead-ion fill at 3.5Z TeV. The spacing of main bunches was 500 ns. Integration time was 250 s. Corrections for detector deadtime and afterpulsing have been applied. Above: Full ring profile showing all present bunches. Due to an offset in the synchronization signal, bunch one appears on the far right, preceded by the abort gap. Below: zoom on the first bunch.
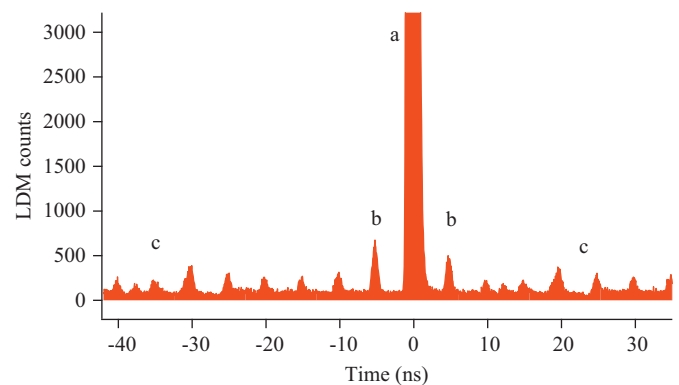

Fig. 8. Typical pattern of satellites in an LHC proton fill, measured at 3.5 TeV. The spacing of main bunches was 50 ns. Integration time was 500 s. (a) Main bunch with peak at 2.5×10^5 counts. (b) Satellite bunches with 5 ns spacing. (c) Ghost bunches are mostly formed in the SPS and occur with 5 ns spacing, with a few small ghosts at 2.5 s spacing.

To illustrate the large dynamic range that can be achieved with correction, examples of typical profiles for both protons and heavy ions are shown in Figs. 8 and 9. Ghost bunches can be distinguished with a dynamic range of more than 10^4. In the case of protons, almost all the satellites are spaced at 5 ns intervals, and are thought to originate in the LHC injector chain where a 200 MHz RF frequency, corresponding to this 5 ns bucket spacing, is used. In the case of heavy ions, in addition to the larger 5 ns satellites near to the full bunch, small ghost bunches can be seen spaced at 2.5 ns intervals (i.e. occupying the 400 MHz LHC RF buckets) and spread around the ring with the population slowly decreasing far from the main bunches. This pattern of satellites,

with the largest occurring 15 ns before the bunch, was reproduced in most lead ion fills.

The importance of correction in obtaining an accurate longitudinal profile is shown in Fig. 10. Without correction, the noise caused by afterpulsing is comparable to the satellites, and the satellites following the main bunch are clearly suppressed by the detector deadtime.

5. Comparison with existing instruments

5.1. Bunch currents

Absolute intensity calibration of the LDM is complicated by the dependence of synchrotron light production on beam energy and by the dependence of the light coupling efficiency into the detector on the precise steering of the BSRT mirrors. However, the relative population of all bunches in the LHC ring can be easily extracted and compared to that measured by the fast beam current transformer (BCT) [27]. The fast BCT measures the beam charge by detecting the current induced by the beam in a secondary winding around a transformer core of high permeability material. Acquisition electronics then integrates all charges in 25 ns time slots. The LDM can therefore reproduce these bunch currents simply by re-binning the histogram into 25 ns bins.

Such a comparison is shown in Fig. 11. Since bunches are injected sequentially, the first bunches have been circulating for longer and thus have a smaller current due to gradual losses. There is very good agreement between BCT and LDM on the relative current in neighboring bunches. However, there is a trend over the whole ring in which the LDM measures too little current at the end (or too much at the beginning) relative to the fast BCT. The discrepancy is approximately $\pm 5\%$ and points to a systematic effect. The difference is greater when the LDM is run at higher count rates, showing that it is responsible for the majority of the difference. While an error in the correction algorithm cannot be
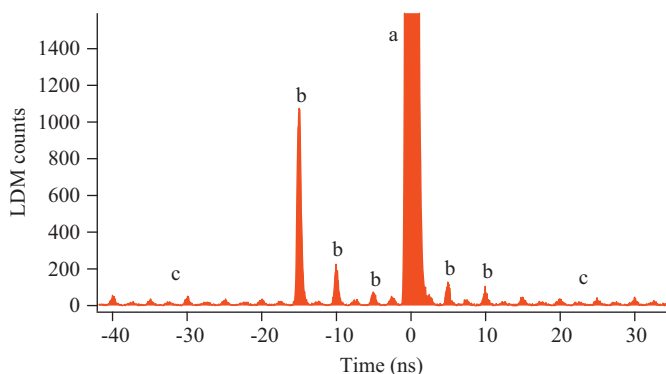

Fig. 9. Typical pattern of satellites in an LHC lead ion fill, measured at 3.5Z TeV. The spacing of main bunches was 500 ns. Integration time was 250 s. (a) Main bunch with peak at 1.29×10^5 counts. (b) Satellite bunches with 5 ns spacing, assumed to originate in the injector chain. (c) Ghost bunches with 2.5 ns spacing, caused by debunched beam captured in the empty RF buckets.
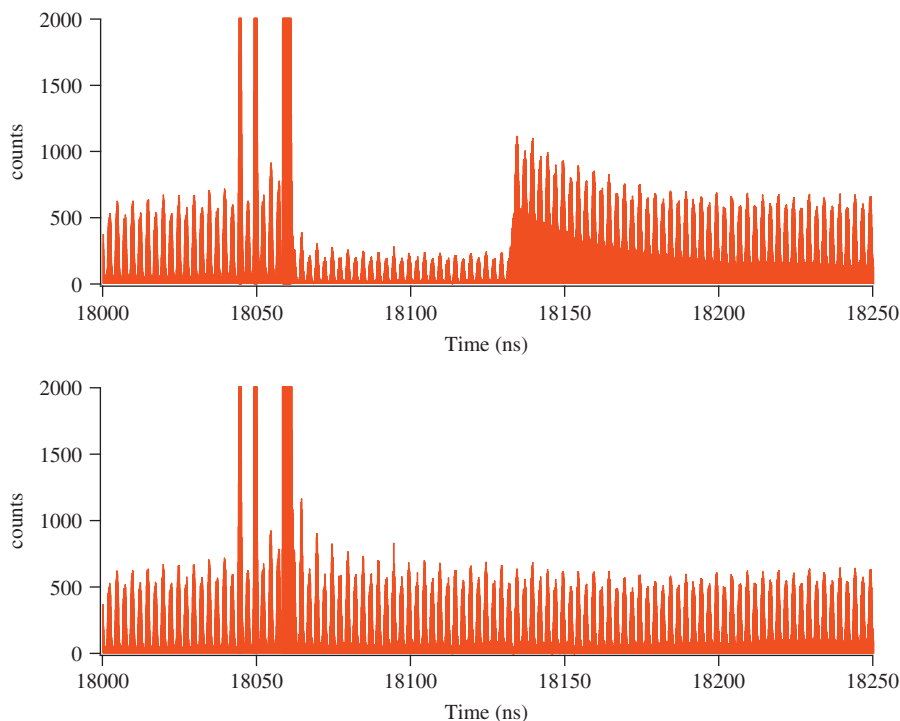

Fig. 10. Correction for afterpulsing and deadtime. Lead ions with 500 ns bunch spacing. The main bunch (peak 950,000 counts) arrives at 18,060 ns and is preceded by two satellites (peaks 5000 and 9000 counts); ghost bunches spaced at 2.5 ns are present throughout the ring. Above: raw signal. The count rate is reduced immediately after the bunch for 77 ns (deadtime) after which sensitivity is restored and the noise level increases (afterpulsing). Below: corrected signal.
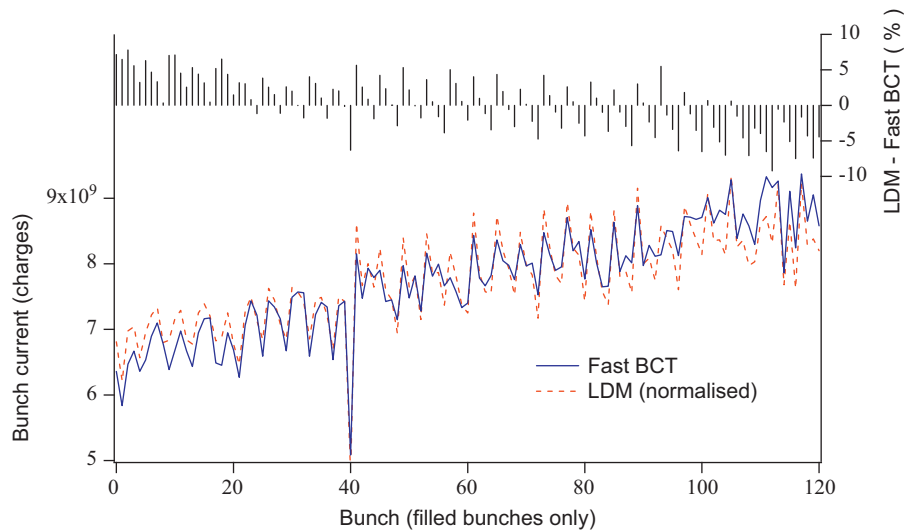
Fig. 11. Bunch currents measured by the LDM and the fast beam current transformer (BCT). The ring was filled with 121 bunches of lead ions at 3.5*Z* TeV with minimum spacing of 500 ns. The LDM produces only relative bunch currents and the sum of the bunch currents has been normalized to the fast BCT sum. Below and left axis, measured bunch currents. Above and right axis, difference in the two measurements, showing a clear trend.
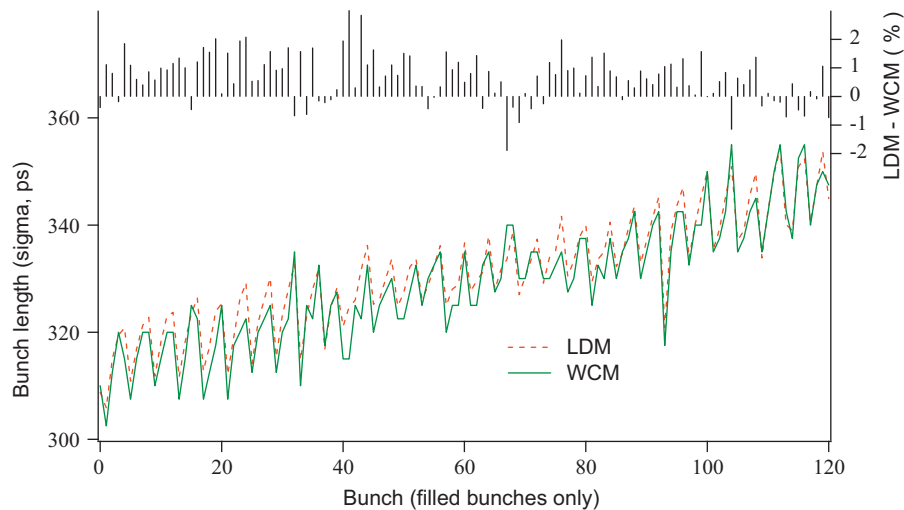

Fig. 12. Bunch lengths measured by the LDM and the wall current monitor (WCM). The ring contained 121 bunches of lead ions at 3.5*Z* TeV with minimum spacing of 500 ns. The LDM jitter of 90 ps is subtracted in quadrature from the measured bunch length. Below and left axis, measured bunch lengths. Above and right axis, difference in the two measurements.

excluded, it seems that some unknown dependency of the APD module may be responsible, such as a change in the sensitivity or the deadtime length with increased count rate. These possibilities are currently being investigated.

5.2. Bunch lengths

The profile obtained by the LDM can also be used to determine individual bunch lengths. In this case, a high dynamic range is not necessary and an integration time of 10 s is sufficient. A Gaussian fit is applied to each bunch. The bunch lengths thus obtained are compared with those measured by the LHC wall current monitor, sometimes known as the Beam Quality Monitor, in Fig. 12. The LDM is estimated to have a jitter of $\sigma = 90$ ps mainly composed of START pulse jitter, $\sigma = 75$ ps, the resolution of the PDM, $\sigma = 50$ ps, and the quantization error due to binning, $\sigma = 15$ ps. This is subtracted in quadrature from the σ given by the Gaussian fit. The wall current monitor provides a single measurement taken every 5 s and digitized at 8 GSamples/s. The FWHM bunch length

is calculated by interpolation of samples lying above and below half maximum. This is converted to σ assuming that the bunch is Gaussian and a subtraction is made to account for dispersion in the pickup and cables. The agreement is very close around the whole ring.

6. Outlook

An LDM has now been installed on the second LHC beam and began taking data since March 2011. For comparison, a different detector has been used, the id100 module from idQuantique. This detector exhibits lower rates of afterpulsing and dark counts. However, it suffers from a long tail in its response caused by absorption of the photon outside the active layer of the silicon and slow diffusion of the avalanche into the active region. While 99% of incident photons are detected with good time resolution, the rest can be detected several ns after their arrival. This tail was sufficient to make the data from 5 buckets following the main

bunch unusable. For this reason it has been decided to replace the id100 with a second PDM module.

A number of further improvements for the LDM are foreseen. The LDM has already demonstrated its potential for machine optimization and software is now being developed so that LDM data is available to LHC operators on-line and automatically logged for future reference.

The APDs used for the LDMs have a small active area of 50 μm diameter. Steering of the synchrotron light is therefore crucial. In order to be independent of the other BSRT instruments, it is planned to mount the APDs on an *XY* translation stage that can be controlled remotely. In addition, an optical diffuser and a condensing lens may be added in order to eliminate any dependence of the LDM on the transverse size of the beam.

Previously, an attempt was made to couple the synchrotron light into an optical fiber and transport it to a fiber-coupled APD located outside the tunnel. The results were not good due to poor coupling efficiency and dispersion in the fiber. However, further investigation into this method is also planned.

The photon counting method is highly sensitive to jitter in the clock pulse. At present, the LDM resolution is limited by the turn clock jitter with $\sigma = 75$ ps. A more accurate turn clock is available from the RF cavities and an optical link to send this to the LDM will be installed soon.

7. Conclusion

It has been shown that a photon-counting method can produce high-resolution longitudinal beam profiles. The method is suitable for the low intensity synchrotron light found in high energy hadron accelerators and has been demonstrated with both protons and heavy ions. A high count rate, and consequently a shorter integration time, can be used provided that suitable correction is applied. Although the results are so far mostly qualitative, it has been shown that the statistical subtraction of afterpulses allows a high dynamic range of up to 10^5 with an integration time of a few minutes. Work remains to be done to fine-tune the correction parameters, which depend on the probability of afterpulsing with respect to time. Ultimately the dynamic range is limited by the uncertainty in the determination of this probability and its stability at varying count rates.

Early results from the LHC Longitudinal Density Monitor show that the data obtained are in good agreement with existing instruments, but largely exceed them in sensitivity. It has already proven itself as a useful tool for beam physics and machine optimization.

References

[1] O. Bruning, P. Collier, P. Lebrun, S. Myers, R. Ostojic, J. Poole, P. Proudlock, LHC Design Report, Geneva, 2004.
[2] M. Benedikt, R. Cappi, M. Chanel, R. Garoby, M. Giovannozzi, S. Hancock, M. Martini, E. Métral, G. Metral, K. Schindl, in: Proceedings of HEACC, Tsukuba, 2001.
[3] A. Beuret, J. Borburgh, A. Blas, H. Burkhardt, C. Carli, M. Chanel, A. Fowler, M. Gourber-Pace, S. Hancock, M. Hourican, in: Proceedings of EPAC, Lucerne, 2004, pp. 1153–1155.
[4] S. Takano, in: Proceedings of IPAC, Kyoto, 2010, pp. 2392–2396.
[5] G. Kube, in: Proceedings of DIPAC, Venice, 2007, pp. 6–10.
[6] J.M. Byrd, S. De Santis, R. Thurman-Keup, , in: Proceedings of BIW, Fermilab, 2006, pp. 262–270.
[7] G. Kube, G. Priebe, C. Wiebers, K. Wittenburg, in: Proceedings of BIW, Fermilab, 2006, pp. 374–383.
[8] K. Scheidt, in: Proceedings of EPAC, Vienna, (2000), p. 182.
[9] C.P. Welsch, H.H. Braun, E. Bravin, R. Corsini, S. Dobert, T. Lefevre, F. Tecker, P. Urschutz, B. Buonomo, O. Coiro, A. Ghigo, B. Preger, Journal of Instrumentation 1 P09002, (2006).
[10] J.-F. Beche, J. Byrd, S. De Santis, P. Denes, M. Placidi, W. Turner, M. Zolotorev, in: Proceedings of BIW, Knoxville, 2004, pp. 112–119.
[11] B.X. Yang, W.E. Norum, S. Shoaf, J. Stevens, in; Proceedings of BIW, Santa Fe, 2010, pp. 238–242.
[12] P. Odier, in: Proceedings of DIPAC, Mainz, 2003, pp. 216–218.
[13] P. Strehl, Beam instrumentation and diagnostics, Birkhäuser (2006) 33–52.
[14] A. Jeff, S. Bart Pedersen, A. Boccardi, E. Bravin, A.S. Fisher, A. Guerrero Ollacarizqueta, T. Lefevre, A. Rabiller, C.P. Welsch, in: Proceedings of SPIE Photonics, Brussels, 2010, p. 7726.
[15] O. Chubar, P. Elleaume, in: Proceedings of EPAC, Stockholm, 1998, p. 1177.
[16] A. Fisher, A. Goldblatt, T. Lefevre, in: Proceedings of DIPAC, Basel, 2009, pp. 5–7.
[17] E. Bravin, G. Burtin, A. Fisher, A. Guerrero, A. Jeff, T. Lefevre, A. Rabiller, F. Roncarolo, in: Proceedings of IPAC, Kyoto, 2010, pp. 1104–1106.
[18] T. Lefevre, S. Bart Pedersen, A. Boccardi, E. Bravin, A. Jeff, A. Goldblatt, F. Roncarolo, A.S. Fisher, in: Proceedings of IPAC, Kyoto, 2010, pp. 2863–2865.
[19] K. Wille, The Physics of Particle Accelerators: An Introduction, Oxford University Press, 1996, pp. 37–38.
[20] ⟨www.microphotondevices.com/products_pdm.asp⟩, accessed 24/06/2011.
[21] A.D. Renker, Nuclear. Instrumentation. and Methods in Physics Research. A 567 (2006) 48.
[22] ⟨www.agilent.com⟩, accessed 24/06/2011.
[23] B.G. Taylor, in: Proceedings of the Eighth Workshop on Electronics For LHC Experiments, Colmar, 2002, pp. 9–13.
[24] E. Bravin, Dead Time Effects on Single Photon Counting For the Longitudinal Density Monitor of LHC, CERN note AB-2006-017 BI, Geneva, 2006.
[25] K. Jensen, et al., Applied Physics Letters 88 (2006) 133503.
[26] M. Ghioni, A. Gulinatti, I. Rech, F. Zappa, S. Cova, IEEE Journal of Selected Topics in Quantum Electronics 13 (2007) 852.
[27] D. Belohrad, J.-j Gras, L.K. Jensen, O.R. Jones, M. Ludwig, P. Odier, J.J. Savioz, S. Thoulet, in: Proceedings of the IPAC, Kyoto, 2010, pp. 1110–1112.